Journal of the Brazilian Society of Mechanical Sciences and Engineering (2018) 40:521
https://doi.org/10.1007/s40430-018-1429-5

REVIEW

Behavior of stratifications and convective phenomena in mixed convection flow of 3D Carreau nanofluid with radiative heat flux

M. Irfan[1] · M. Khan[1] · W. A. Khan[2]

Received: 27 May 2018 / Accepted: 19 September 2018 / Published online: 13 October 2018

Abstract
Nanoliquids, the engineered liquids with isolated effectual nanoparticles have disclosed a surprising thermo-physical effects and added functionalities and therefore have supported an extensive sort of essential applications. In particular, nanoliquids have displayed pointedly improved aptitude of heat transfer as equated to traditional functioning liquids. The notable intention of current scrutiny is to explore the features of combined convective and stratification phenomena by utilizing Brownian and thermophoresis nanoparticles on 3D mixed convection flow of magnetite Carreau fluid influenced by a bidirectional stretching surface. The heat transport phenomenon is also betrothed in the manifestation of thermal radiation and the heat sink/source. By means of suitable conversions the nonlinear PDEs transformed into nonlinear ODEs. To identify the behavior of numerous somatic parameters, numerically bvp4c tactic has been worked to elucidate the governing ODEs. The graphical depiction is delineated and tables are organized for diverse physical parameters on Carreau nanofluid. It is scrutinized that the impact of magnetic parameter on both the velocity components is analogous and diminishes both the velocities for shear thinning/thickening liquids. Moreover, the present exploration reports that the mixed convection and thermal stratification parameters decline the liquid temperature and allied thickness of the thermal boundary layer for both shear thickening/thinning liquids.

Keywords 3D Carreau nanofluid · Mixed convection · Thermal radiation · Heat sink/source · Double stratification · Combined convective conditions

List of symbols

$\mathbf{S}^*$	Cauchy stress tensor
p	Pressure
$\mathbf{I}$	Identity tensor
$\dot{\gamma}$	Shear rate
Γ	Material rate constant
(μ_0, μ_∞)	Zero and infinity shear rate viscosities
$\mathbf{A}_1$	First Rivlin–Ericksen tensor
n	Power law index
u, v, w	Velocity components
x, y, z	Space coordinates
ν	Kinematic viscosity
σ	Electrical conductivity
ρ_f	Fluid density
B_0	Strength of magnetic field
g	Gravitational acceleration
α_1	Thermal diffusivity
k	Nanofluid thermal conductivity
(β_T, β_C)	Thermal and concentration coefficients expansion
(T, C)	Temperature and concentration of fluid
τ	Effective heat capacity ratio
D_{B}	Brownian diffusion coefficient
D_{T}	Thermophoresis diffusion coefficient
(T_∞, C_∞)	Nanofluid ambient temperature and concentration
(T_0, C_0)	Reference temperature and concentration
(d, d_1, e, e_1)	Dimensionless constants
q_r	Radiative heat flux
k^*	Mean absorption coefficient
σ^*	Stefan–Boltzmann constant
Q_0	Heat source/sink coefficient
$U_w(x),\ V_w(x)$	Stretching velocities
a, b	Positive constants
(h_f, h_m)	Heat and mass wall transfer coefficient

Technical Editor: Cezar Negrao.

✉ M. Irfan
mirfan@math.qau.edu.pk

[1] Department of Mathematics, Quaid-i-Azam University, Islamabad 44000, Pakistan

[2] Department of Mathematics and Statistics, Hazara University, Mansehra 21300, Pakistan

$\left(T_f, C_f\right)$	Heated fluid temperature and concentration
η	Dimensionless variable
(We_1, We_2)	Local Weissenberg numbers
M	Magnetic parameter
λ^*	Mixed convection parameter
N^*	Buoyancy ratio parameter
R	Thermal radiation
(S_1, S_2)	Thermal and mass stratification parameters
(γ_1, γ_2)	Thermal and mass Biot numbers
N_{b}	Brownian motion parameter
N_{t}	Thermophoresis parameter
δ	Heat source/sink parameter
Le	Lewis number
α	Ratio of stretching rates parameter
(τ_{xz}, τ_{yz})	Surface shear stresses along x- and y-directions
(C_{fx}, C_{fy})	Skin friction coefficients
$\left(Nu_x, Sh_x\right)$	Local Nusselt and Sherwood numbers
Re_x	Local Reynolds number
(f, g)	Dimensionless velocities
θ	Dimensionless temperature
φ	Dimensionless concentration

Abbreviations

ODEs	Ordinary differential equations
PDEs	Partial differential equations
3D	Three dimensional

1 Introduction

Energy disaster instigated by the hurried world population and engineering progression in addition to the rapid expansion of the society intensifies gradually and might develop a humanitarian disaster in worldwide. Solar energy has been demanded as the energy of our forthcoming, but approaches with many experiments to overcome, for instance, the high cost and the low proficiency. Solar thermal structure, which usually has a fascinating plate with liquid running inside the pipes, is a communal approach of consuming solar energy. Its competence is partial by not only how competently the solar energy is caught by the fascinating plate, but also how effectually the fascinated energy is transported to the running liquid. Solar energy is the utmost essential renewable cause of energy to produce heat and electrical energy. Countless solar constructed thermal structures are used for producing water distillation, heating of water from solar radiation, electricity and structures air-conditioning. Moreover, the enhancing process of heat transfer in solar energy structures is solitary of the utmost crucial subjects to attain an enhanced enactment of these structures with dense strategies. This might be attained by means of functioning liquids with boosted thermo-physical chattels. One of the operative approaches is to substitute the functioning liquid with nanoliquids as an innovative approach to develop the heat transfer features of the liquid.

In current spans, the rapid expansion in engineering and thermal industrial progressions necessitates additional dense and proficient heat transport structures. In these structures, fluids are utilized as cooling instrument. Owing to lesser in thermal conductivity, these liquids critically disturb the amount of heat transport or cooling progression. It was a thought-provoking assignment to heighten the liquid thermal conductivity for scientists and investigators. Here originates the notion of nanofluids. Nanofluids are as innovative novelty, which was first proposed by Choi [1]. The deferral of nonmetallic and metallic nanoparticles in base liquids like aquatic and paraffin is known as nanofluid. They exhibit boosted thermo-physical assets, equated to base liquids. The manifestation of nanomaterials in the base liquids provides an enhanced flow of fraternization and sophisticated thermal conductivity equated to purify liquids. There are numerous norms with nanotechnology in industrial-related diligences. This innovative expertise is frequently exploited in the creation of nanochips, chilling of microchip technology, lorries apparatus, exchange making, medication distribution, etc. Additionally, the thermal assets of nanoliquids are the assets which are very essential to nanofluids enactment. These are the liquid thermal conductivity, viscosity, specific heat and heat transfer coefficient, respectively. Thermal recital of solar collectors is essentially being contingent on how thermal assets perform in diverse functioning circumstances. Some of the current reports in these trends can be quantified via refs. [2–12]. The impact of thermal energy and melting heat on radiative flow of carbon–water nanofluid was scrutinized numerically by Hayat et al. [13] by seeing the stagnation point effect. Irfan et al. [14] explored numerically the properties of shear thinning/thickening liquids on 3D Carreau nanofluid flow with the influence of heat sink/source and temperature-dependent thermal conductivity. They inspected that the tendency of unsteadiness and thermal conductivity parameters were quite conflicted for both shear thickening/thinning liquids on temperature and concentration fields. The heat transport phenomenon on unsteady Carreau magneto nanofluid towards the cone packed with alloy nanomaterials was discussed Raju et al. [15]. They reported that the heat transfer amount heightened for the viscous variation parameter. Recently, Hayat et al. [16] investigated fluid flow of magneto nanoliquid subject to nonlinear stretched surface. They analyzed that the pressure and velocity fields decline for power law index. The convective and activation energy phenomena on the flow of nanofluid with the properties of chemical reaction were explored by Zeeshan et al. [17]. The behavior of variable conductivity in Eyring and Carreau fluids with nickel and dust nanoparticles was scrutinized by Upadhya et al. [18].

Recently, the mixed convection transport of non-Newtonian liquids via thermal and solute stratifications is a subject of abundant scrutiny owing to their widespread manifestation in the engineering and industrial progressions. The heat dismissal into the atmosphere, for instance, streams, oceans and ponds, and thermal energy-storing structures like astrophysical pools are the numerous specimens of such solicitations. Stratification of liquid is a deposition or establishment of layers that happens because of temperature changes, concentration variation or owing to the manifestation of diverse liquids. It is fascinating to scrutinize the impact of double stratification when both heat and mass transfer are existing instantaneously. Moreover, in the manifestation of gravity the density dissimilarities have a strategic role in the mixing of heterogeneous liquid and dynamics. For instance, thermal stratification in pools can condense the fraternization of oxygen to the lowest water to become anxious through the achievement of organic progressions. Similarly, the scrutiny of thermal stratification is essential for the solar industry as greater energy competence can be attained with enhanced stratification. The mixed convection thermally stratified flow along a stretched cylinder was scrutinized by Mukhopadhyay and Ishak [19]. The stimulus of chemically reacting flow and mixed convective on nanoliquid toward the moving surface was analyzed by Mahantesh et al. [20]. Imtiaz et al. [21] considered the effects of mixed convection and convective phenomena on Casson nanofluid due to stretched cylinder. They examined that for larger Casson liquid and magnetic parameters decline the liquid flow. Waqas et al. [22] explored the mutual effects of thermal and mass stratification on mixed convection Oldroyd-B nanoliquid. They reported that the higher thermal and solutal stratified causes decline the temperature and concentration field, respectively. Moreover, current endeavors on mixed convection as well as double stratifications via diverse thoughtfulness can be referred through refs. [23–26].

In numerous applications, non-Newtonian materials have sizeable worth throughout the earliest limited spans. In these materials, there is no linear correlation between stress tensor and deformation. The remarkable features of these liquids are their advanced apparent viscosities; therefore, laminar flow circumstances intensify considerably compared to Newtonian liquids. The applications correlated to biological progressions, geophysics and genetic disciplines comprise non-Newtonian ingredients. These materials, for instance, bubbles, colloidal and deferral elucidations, adhesives, stone undercoat and soap suds are nonlinear materials. Numerous researchers have functioned with diverse non-Newtonian liquids which can be seen in refs. [27–34].

In this scrutiny, numerical elucidations are established for 3D radiative flow of a magnetite Carreau nanofluid subject to combined phenomena of convective and stratification influenced by stretching surface. The impact of the heat sink/source is also considered. A compatible conversion changed the PDEs into ODEs and then elucidated numerically by bvp4c to scrutinize the features of physical parameters. Graphs are structured and tables are established and conferred it details.

2 Physical model and constitutive relation

2.1 Rheological models

This study scrutinized Carreau fluid model which is a generalized Newtonian liquid that describes the properties of shear thinning/thickening liquids. The Cauchy stress tensor for the Carreau fluid model is stated as [35–38]:

$$\mathbf{S}^{*}= -p\mathbf{I}+\mu(\dot{\gamma})\mathbf{A}_1, \tag{1}$$

with

$$\mu(\dot{\gamma}) = \mu_\infty + (\mu_0 - \mu_\infty)[1 + (\Gamma\dot{\gamma})^2]^{\frac{n-1}{2}}, \tag{2}$$

where $(p, \mathbf{I}, \Gamma, n, \mu_0, \mu_\infty)$ are the pressure, identity tensor, material time constant, power law index, zero-shear rate and infinity shear rate viscosities, respectively.

Furthermore, the shear rate and first Rivlin–Ericksen tensor A_1 is defined as:

$$\dot{\gamma} = \sqrt{\frac{1}{2}tr(\mathbf{A}_1^2)}, \quad \mathbf{A}_1 = \nabla\mathbf{V} + (\nabla\mathbf{V})^T. \tag{3}$$

We consider the most useful conditions, i.e., $\mu_0 >> \mu_\infty$ and $\mu_\infty = 0$. Thus, in view of Eqs. (2), (1) reduces to following form we have

$$\mathbf{S}^{*}= -p\mathbf{I}+\mu_0[1 + (\Gamma\dot{\gamma})^2]^{\frac{n-1}{2}}\mathbf{A}_1. \tag{4}$$

Furthermore, for $n > 1$ this model describes the effects of shear thickening fluid, while for $0 < n < 1$ the effects of shear thinning fluid are attained.

For incompressible 3D fluid flow, the velocity, temperature, concentration and the Cauchy stress tensor are assumed to be:

$$\begin{aligned}&\mathbf{V} = [u(x,y,z),\ v(x,y,z),\ w(x,y,z)],\\ &T = T(x,y,z), \quad C = C(x,y,z), \quad \mathbf{S}^{*}= \mathbf{S}^{*}(x,y,z).\end{aligned} \tag{5}$$

Here (u, v, w) are the velocity components in x-, y- and z-directions.

2.2 Governing equations

The constitutive equations for incompressible 3D time-independent flow of Carreau fluid [37] in vectorial form are represented as:

$$\text{div } \mathbf{V} = 0, \tag{6}$$

$$\rho_f(\mathbf{V}\cdot\nabla) = \nabla\cdot\mathbf{S}^*, \tag{7}$$

where ρ_f is the fluid density.

Utilizing Eq. (5) in Eqs. (6) and (7), having in mind Eqs. (3) and (4), a lengthy but forthright scheme gives the following boundary layer equation as follows:

$$\frac{\partial u}{\partial x} + \frac{\partial v}{\partial y} + \frac{\partial w}{\partial z} = 0, \tag{8}$$

$$u\frac{\partial u}{\partial x} + v\frac{\partial u}{\partial y} + w\frac{\partial u}{\partial z} = -\frac{1}{\rho_f}\frac{\partial p}{\partial x} + \nu\frac{\partial^2 u}{\partial z^2}\left[1+\Gamma^2\left(\frac{\partial u}{\partial z}\right)^2\right]^{\frac{n-1}{2}} + \nu\left(\frac{\partial u}{\partial z}\right)\frac{\partial}{\partial z}\left[1+\Gamma^2\left(\frac{\partial u}{\partial z}\right)^2\right]^{\frac{n-1}{2}}, \tag{9}$$

$$u\frac{\partial v}{\partial x} + v\frac{\partial v}{\partial y} + w\frac{\partial v}{\partial z} = -\frac{1}{\rho_f}\frac{\partial p}{\partial y} + \nu\frac{\partial^2 v}{\partial z^2}\left[1+\Gamma^2\left(\frac{\partial v}{\partial z}\right)^2\right]^{\frac{n-1}{2}} + \nu\left(\frac{\partial v}{\partial z}\right)\frac{\partial}{\partial z}\left[1+\Gamma^2\left(\frac{\partial v}{\partial z}\right)^2\right]^{\frac{n-1}{2}}, \tag{10}$$

$$0 = -\frac{1}{\rho_f}\frac{\partial p}{\partial z}, \tag{11}$$

where ν is the kinematic viscosity.

3 Problem Formulation

We scrutinize the steady 3D mixed convection flow of a Carreau magnetite nanofluid over a bidirectional stretched surface. The influence of combined stratification and convective conditions is engaged in heat and mass transfer phenomena. Additionally, thermal radiation and the heat sink/source are deliberated. The Brownian motion and thermophoresis nanoparticles are also betrothed in this study. The flow is persuaded by stretching the surface in two nearby x- and y-directions with linear velocity $(u, v) = (ax, by)$, respectively, where a, $b > 0$ and the fluid overcomes the region $z > 0$. Furthermore, it is also supposed that the electric and magnetic fields are negligible when we equated with applied magnetic field (as depicted in Fig. 1). This notion is only effective when the magnetic Reynolds number is small.

Under these attentions, the governing problem of magnetite Carreau nanofluid is:

$$\frac{\partial u}{\partial x} + \frac{\partial v}{\partial y} + \frac{\partial w}{\partial z} = 0, \tag{12}$$

$$u\frac{\partial u}{\partial x} + v\frac{\partial u}{\partial y} + w\frac{\partial u}{\partial z} = \nu\frac{\partial^2 u}{\partial z^2}\left[1+\Gamma^2\left(\frac{\partial u}{\partial z}\right)^2\right]^{\frac{n-1}{2}} + \nu(n-1)\Gamma^2\left(\frac{\partial u}{\partial z}\right)^2\frac{\partial^2 u}{\partial z^2}\left[1+\Gamma^2\left(\frac{\partial u}{\partial z}\right)^2\right]^{\frac{n-3}{2}} - \frac{\sigma B_0^2}{\rho_f}u + g[\beta_T(T-T_\infty) + \beta_C(C-C_\infty)], \tag{13}$$

$$u\frac{\partial v}{\partial x} + v\frac{\partial v}{\partial y} + w\frac{\partial v}{\partial z} = \nu\frac{\partial^2 v}{\partial z^2}\left[1+\Gamma^2\left(\frac{\partial v}{\partial z}\right)^2\right]^{\frac{n-1}{2}} + \nu(n-1)\Gamma^2\left(\frac{\partial v}{\partial z}\right)^2\frac{\partial^2 v}{\partial z^2}\left[1+\Gamma^2\left(\frac{\partial v}{\partial z}\right)^2\right]^{\frac{n-3}{2}} - \frac{\sigma B_0^2}{\rho_f}v, \tag{14}$$

$$u\frac{\partial T}{\partial x} + v\frac{\partial T}{\partial y} + w\frac{\partial T}{\partial z} = \alpha_1\frac{\partial^2 T}{\partial z^2} + \tau\left[D_B\frac{\partial C}{\partial z}\frac{\partial T}{\partial z} + \frac{D_T}{T_\infty}\left(\frac{\partial T}{\partial z}\right)^2\right] - \frac{1}{(\rho c)_f}\frac{\partial q_r}{\partial z} + \frac{Q_0}{(\rho c)_f}(T-T_\infty), \tag{15}$$

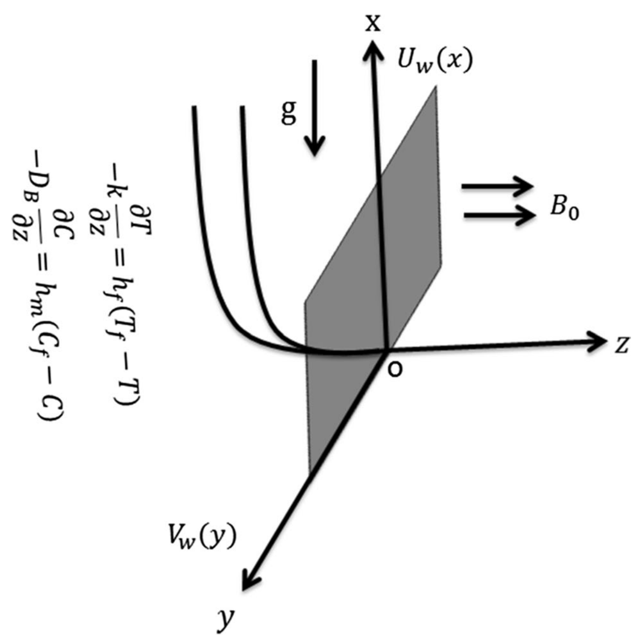

Fig. 1 Flow configuration

$$u\frac{\partial C}{\partial x} + v\frac{\partial C}{\partial y} + w\frac{\partial C}{\partial z} = D_B\frac{\partial^2 C}{\partial z^2} + \frac{D_T}{T_\infty}\frac{\partial^2 T}{\partial z^2}. \tag{16}$$

Subject to the boundary conditions:

$$\begin{aligned} &u = U_w(x) = ax,\ v = V_w(y) = \text{by},\ w = 0,\\ &-k\frac{\partial T}{\partial z} = h_f[T_f - T],\ -D_B\frac{\partial C}{\partial z} = h_m[C_f - C] \text{ at } z = 0, \end{aligned} \tag{17}$$

$$u \to 0,\ v \to 0,\ T \to T_\infty,\ C \to C_\infty \text{ as } z \to \infty. \tag{18}$$

Where B_0 is the strength of magnetic field, σ the electrical conductivity, g the gravitational acceleration, (β_T, β_C) the coefficients of thermal and concentration expansion, respectively, (T, C) the nanoliquid temperature and volume friction, α_1 the thermal diffusivity of liquid, k thermal conductivity of fluid, (ρ_f, c_f) the liquid density and specific heat, respectively, τ the ratio of effective heat capacity of nanoparticles to heat capacity of the base liquid, Q_0 the heat sink/source coefficient, (D_B, D_T) the Brownian and thermal diffusion coefficients, respectively. Furthermore, (h_f, h_m) are the variable wall heat and variable wall mass transfer coefficients, respectively, $(T_f, C_f) = (T_0 + \mathrm{d}x, C_0 + ex)$ the heated liquid temperature and concentration, respectively, $(T_\infty, C_\infty) = (T_0 + d_1x, C_0 + e_1x)$ the ambient temperature and concentration, respectively, in which $(T_0,\ C_0)$ the reference temperature and concentration, respectively, $(d,\ d_1,\ e,\ e_1)$ the dimensionless constants and q_r the radiative heat flux which is defined as

$$q_r = \frac{-16\sigma^* T_\infty^3}{3k^*}\frac{\partial T}{\partial z}, \tag{19}$$

in which (σ^*, k^*) are the Stefan–Boltzmann constant and mean absorption coefficient, respectively.

3.1 Appropriate conversions

$$\begin{aligned} &u = axf'(\eta),\ v = ayg'(\eta),\ w = -\sqrt{av}[f(\eta) + g(\eta)],\\ &\theta(\eta) = \frac{T - T_\infty}{T_f - T_0},\ \varphi = \frac{C - C_\infty}{C_f - C_0},\ \eta = z\sqrt{\frac{a}{v}}. \end{aligned} \tag{20}$$

In vision of above conversions, Eq. (12) is satisfied automatically and Eqs. (13–18) are reduced to the following ODEs:

$$\begin{aligned} &f'''\left[1 + We_1^2 f''^2\right]^{\frac{n-3}{2}}\left[1 + nWe_1^2 f''^2\right]\\ &-f'^2 + f''(f+g) - M^2 f' + \lambda^*(\theta + N^*\varphi) = 0, \end{aligned} \tag{21}$$

$$g'''\left[1 + We_2^2 g''^2\right]^{\frac{n-3}{2}}\left[1 + nWe_2^2 g''^2\right] - g'^2 + g''(f+g) - M^2 g' = 0, \tag{22}$$

$$\begin{aligned} &\left(1 + \frac{4}{3}R\right)\theta'' + Pr(f+g)\theta' - Prf'\theta - Pr\,S_1 f'\\ &+ Pr\left[N_b\theta'\varphi' + N_t\theta'^2 + \delta\theta\right] = 0, \end{aligned} \tag{23}$$

$$\varphi'' + Pr\,Le(f+g)\varphi' - Pr\,Lef'\varphi - Pr\,LeS_2 f' + \left(\frac{N_t}{N_b}\right)\theta'' = 0, \tag{24}$$

$$\begin{aligned} &f(0) = 0,\ g(0) = 0,\ f'(0) = 1,\ g'(0) = \alpha,\\ &\theta'(0) = -\gamma_1(1 - S_1 - \theta(0))\ ,\varphi'(0) = -\gamma_2(1 - S_2 - \varphi(0)), \end{aligned} \tag{25}$$

$$f' \to 0,\ g' \to 0,\ \theta \to 0\ ,\varphi \to 0 \text{ as } \eta \to \infty. \tag{26}$$

Here $(We_1,\ We_2)\left(= \sqrt{\frac{\Gamma^2 aU_w^2}{v}},\ \sqrt{\frac{\Gamma^2 aV_w^2}{v}}\right)$ are the local Weissenberg numbers, $M\left(= \sqrt{\frac{\sigma B_0^2}{a\rho_f}}\right)$ the magnetic parameter, $\lambda^*\left(= \frac{g\beta_T d}{a^2}\right)$ the mixed convection parameter, $N^*\left(= \frac{\beta_C.e}{\beta_T d}\right)$ the buoyancy ratio parameter, $R_d\left(= \frac{4\sigma^* T_\infty^3}{3kk^*}\right)$ the thermal radiation parameter, $N_b\left(= \frac{\tau D_B(C_f - C_0)}{v}\right)$ the Brownian motion parameter, $N_t\left(= \frac{D_T(T_f - T_0)}{vT_0}\right)$ the thermophoresis parameter, $Pr\left(= \frac{v}{\alpha_1}\right)$ the Prandtl number, $\delta\left(= \frac{Q_0}{a(\rho c)_f}\right)$ the heat source ($\delta > 0$) and heat sink ($\delta < 0$) parameter, $Le(= \frac{\alpha_1}{D_B})$ the Lewis number, $\alpha\left(= \frac{b}{a}\right)$ the ratio of stretching rates parameter, $(\gamma_1, \gamma_2)\ \left(= \frac{h_f}{k}\sqrt{\frac{v}{a}},\ \frac{h_m}{D_B}\sqrt{\frac{v}{a}}\right)$ the thermal and concentration Biot numbers, respectively and $(S_1,\ S_2)\ \left(= \frac{d_1}{d},\ \frac{e_1}{e}\right)$ the thermal and mass stratification parameters, respectively.

4 Physical quantities

From the industrial and engineering point of view, the essential quantities of physical interest are the skin friction, heat and transfer coefficients which may be defined by the subsequent expression:

$$C_{fx} = \frac{\tau_{xz}}{\frac{1}{2}\rho_f U_w^2},\quad C_{fy} = \frac{\tau_{yz}}{\frac{1}{2}\rho_f U_w^2}, \tag{27}$$

$$Nu_x = \left(-\frac{x}{(T_f - T_\infty)} + \frac{xq_r}{k(T_f - T_\infty)}\right)\frac{\partial T}{\partial z}\bigg|_{z=0},$$
$$Sh_x = -\frac{x}{(C_f - C_\infty)}\frac{\partial C}{\partial z}\bigg|_{z=0}. \tag{28}$$

The above quantity is in the dimensionless forms:

$$\frac{1}{2}C_{fx}Re_x^{\frac{1}{2}} = f''(0)\left[1 + We_1^2 f''^2(0)\right]^{\frac{n-1}{2}}, \ \frac{1}{2}$$
$$\left(\frac{U_w}{V_w}\right)C_{fy}Re_x^{\frac{1}{2}} = g''(0)\left[1 + We_2^2 g''^2(0)\right]^{\frac{n-1}{2}}, \tag{29}$$

$$Re_x^{-\frac{1}{2}}Nu_x = \frac{-\left(1+\frac{4R}{3}\right)\theta'(0)}{1-S_1}, \quad Re_x^{-\frac{1}{2}}Sh_x = -\left(\frac{1}{1-S_2}\right)\varphi'(0), \tag{30}$$

in which $Re_x = \frac{ax^2}{\nu}$ is local Reynolds number.

5 Computational scheme

The nonlinear ODEs (21–24) with boundary conditions (25) and (26) are elucidated numerically via bvp4c scheme. Numerical elucidations of these equations are acquired by switching the governing problem into first-order differential structure.

$$f = y_1,\ f' = y_2,\ f'' = y_3,\ f''' = yy_1, \tag{31}$$

$$g = y_4,\ g' = y_5,\ g'' = y_6,\ g''' = yy_2, \tag{32}$$

$$\theta = y_7,\ \theta' = y_8,\ \theta'' = yy_3, \tag{33}$$

$$\varphi = y_9,\ \varphi' = y_{10},\ \varphi'' = yy_4, \tag{34}$$

$$yy_1 = \frac{-(y_1+y_4)y_3 + y_2^2 + M^2 y_2 - \lambda^*(y_7 + N^* y_9)}{\Lambda_1},$$
$$\Lambda_1 = \left(1 + nWe_1^2 y_3^2\right) * \left(1 + We_1^2 y_3^2\right)^{\frac{n-3}{2}}, \tag{35}$$

$$yy_2 = \frac{-(y_1+y_4)y_6 + y_5^2 + M^2 y_5}{\Lambda_2},$$
$$\Lambda_2 = \left(1 + nWe_2^2 y_6^2\right) * \left(1 + We_2^2 y_6^2\right)^{\frac{n-3}{2}}, \tag{36}$$

$$yy_3 = \frac{-Pr(y_1+y_4)y_8 + Pr\, y_2 y_7 + Pr\, S_1 y_2 - Pr\, N_b y_8 y_{10} - Pr\, N_t y_8^2 - Pr\, \delta y_7}{\Lambda_3},$$
$$\Lambda_3 = \left(1 + \frac{4R}{3}\right), \tag{37}$$

$$yy_4 = -Le\, Pr(y_1+y_4)y_{10} + Pr\, Le y_2 y_9 + Pr\, Le S_2 y_2 y_9 - \frac{N_t}{N_b} yy_3, \tag{38}$$

$$y_1(0) = 0,\ y_2(0) = 1,\ y_2(\infty) = 0, \tag{39}$$

$$y_4(0) = 0,\ y_5(0) = \alpha,\ y_5(\infty) = 0, \tag{40}$$

$$y_8(0) + \gamma_1\left(1 - S_1 - y_7(0)\right) = 0,\ y_7(\infty) = 0, \tag{41}$$

$$y_{10}(0) + \gamma_2\left(1 - S_2 - y_9(0)\right) = 0,\ y_9(\infty) = 0. \tag{42}$$

6 Analysis of results

The notable objective here is to disclose the properties of numerous parameters on mixed convection stratified flow of magnetite Carreau nanofluid subject to convective phenomena. The heat transport mechanism is also considered in manifestation of the heat sink/source and thermal radiation. For this persistence, graphs are planned and tables are structured for diverse parameters and discussed in facts. Additionally, the range of scheming parameters in existent study is taken to be $0 \le M \le 1.5$, $0 \le \lambda^* \le 2.0$, $0.1 \le N^* \le 1.8$, $0.7 \le \gamma_1 \le 1.3, 0 \le S_1 \le 0.3, 0.1 \le N_b \le 1.0, 0.4 \le N_t \le 1.6$, $0 \le R \le 1.2, 0.6 \le \gamma_2 \le 1.5, 0 \le S_2 \le 0.5$.

6.1 Impact of M on $f'(\eta)$ and $g'(\eta)$

To envision the impact of magnetic parameter M on velocity fields $f'(\eta)$ and $g'(\eta)$ for both shear thinning/thickening cases, Fig. 2a–d is strategized. It is noted that both the liquid velocities decline for enhancing the values of M for shear thinning/thickening cases. This occurs because of the circumstance that the outcomes of strong magnetic field contribute resistance to flow in both the x- and y-directions which intensify the Lorentz force in z-direction. Therefore, the flow in both the directions decay the liquid velocities.

6.2 Impact of λ^* and N^* on $f'(\eta)$ and $g'(\eta)$

The stimulus of growing value of mixed convection parameter λ^* and buoyancy ratio parameter N^* on velocity fields for $(n < 1)$ and $(n > 1)$ is schemed in Figs. 3a–d and 4a–d. It is noteworthy to note that when we heighten the value of these parameters the liquid velocity $f'(\eta)$ increases for both ($n = 0.5$ and $n = 1.5$). Physically, augmented values of mixed convection parameter λ^* reason a forceful buoyancy force which clues the escalation of velocity field $f'(\eta)$. Similarly, the concentration buoyancy strength boosts up for the increase in buoyancy ratio parameter N^* which consequence the declinse of the velocity field $g'(\eta)$. Moreover, it is reported that both the velocity fields decay for augmenting values of λ^* and N^* for both $(n < 1)$ and $(n > 1)$ as displayed in Figs. 3c, d and 4c, d. Hence, we can say from these

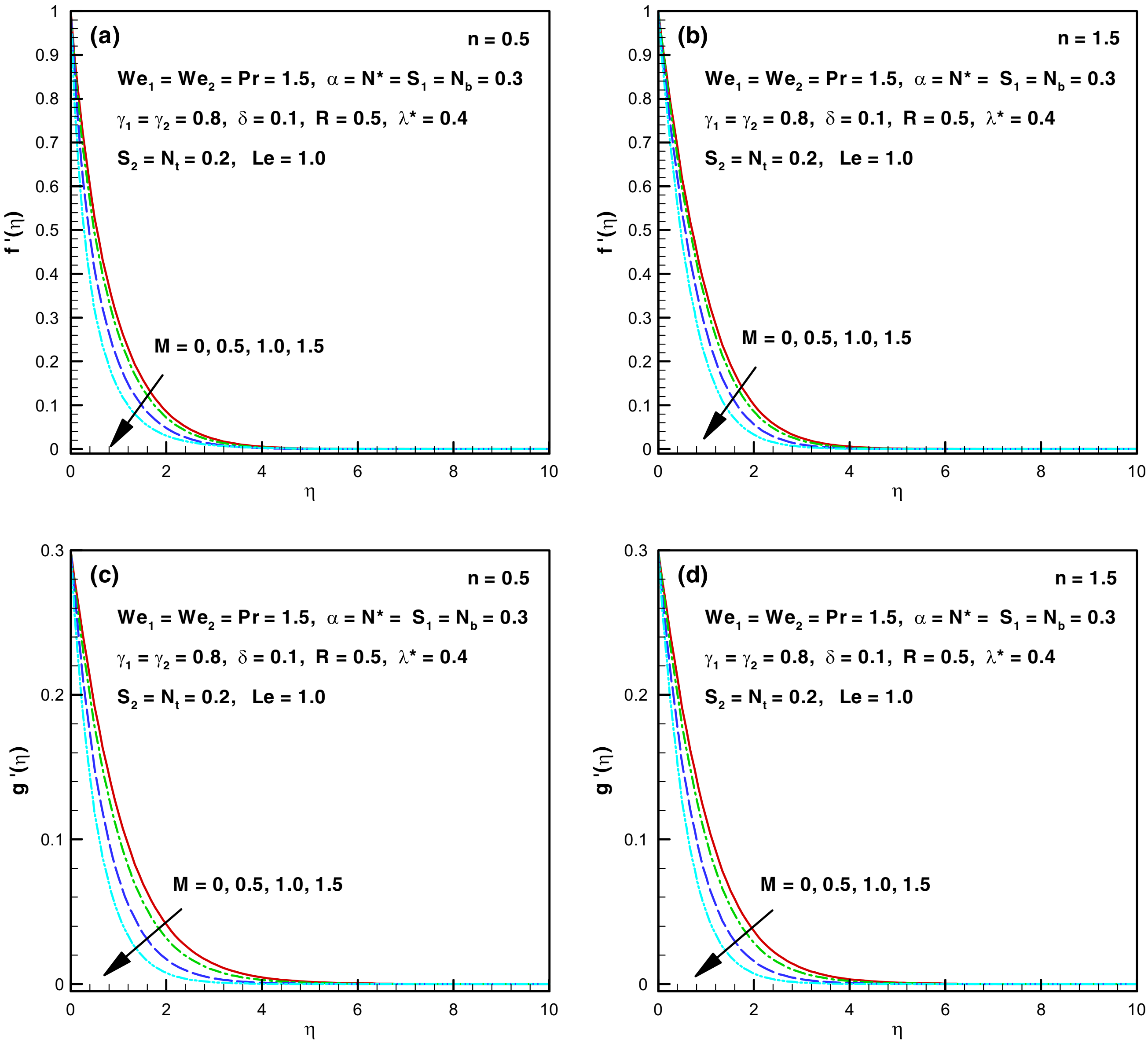

Fig. 2 **a–d** Impact of M on $f'(\eta)$ and $g'(\eta)$

strategies that the impact of these flow parameters is entirely conflicting for velocity field $f'(\eta)$ and $g'(\eta)$.

6.3 Impact of λ^* and N^* on $\theta(\eta)$

Figures 5a, b and 6a, b are intended to visualize the enactment of mixed convection parameter λ^* and buoyancy ratio parameter N^* for shear thickening/thinning cases on nanoliquid temperature field. From these structures, it is scrutinized that both the λ^* and N^* are retreating functions of temperature distribution. For higher value of λ^* and N^* display thinner thickness of the thermal boundary layer and temperature of Carreau nanofluid. The enhancing value of mixed convection parameter λ^* relate to stronger buoyancy force because mixed convection parameter depends on buoyancy force. Hence, this stronger buoyancy force is the reason for the decline in temperature and its allied thickness of the boundary layer. Furthermore, analogous enactment is being detected for the progressive value of buoyancy ratio parameter N^*.

6.4 Impact of γ_1 and S_1 on $\theta(\eta)$

Figures 7a, b and 8a, b expose the tendency of thermal Biot number γ_1 and stratification parameter S_1, respectively, for ($n = 0.5$ and 1.5) on Carreau liquid temperature field. Here we scrutinized that quite conflicting tendency is being famed for growing value of γ_1 and S_1. When we intensify the values

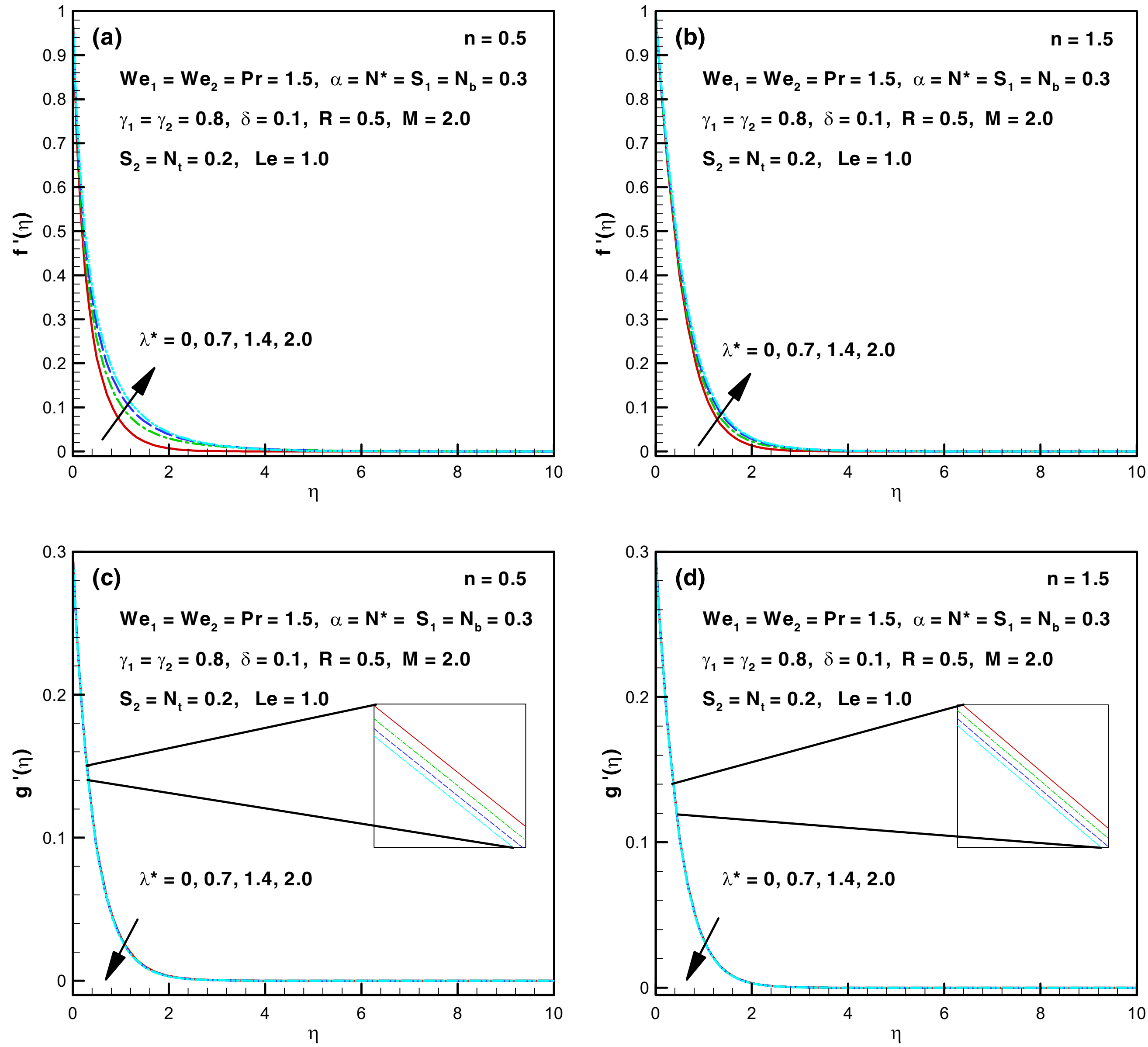

Fig. 3 **a–d** Impact of λ^* on $f'(\eta)$ and $g'(\eta)$

of thermal Biot number γ_1, the temperature field enhances; however, the temperature of Carreau fluid is declining function of thermal stratification parameter S_1. Physically, enlarging the values of thermal Biot number γ_1 rises the heat transfer amount which is responsible to enhance the temperature profile. Moreover, our scrutiny explores that the difference between the sheet and ambient liquid temperature decreases for larger values of S_1. Consequently, the thickness of the thermal boundary layer and temperature field decays for S_1 as shown in Fig. 8a, b.

6.5 Impact of N_b and N_t on $\theta(\eta)$

The nanoparticles display a strategic role for the enhancement of heat transfer features in Carreau fluid. For this persistence, Figs. 9a, b and 10a, b are designed for both ($n < 1$ and $n > 1$). We scrutinized from these drafts that N_b and N_t both are boosting the liquid temperature and thermal thickness of the boundary layer. Intensification in N_b enriching the accidental gesture of liquid particles and additional heat is formed which rises the temperature field. In Fig. 9a,

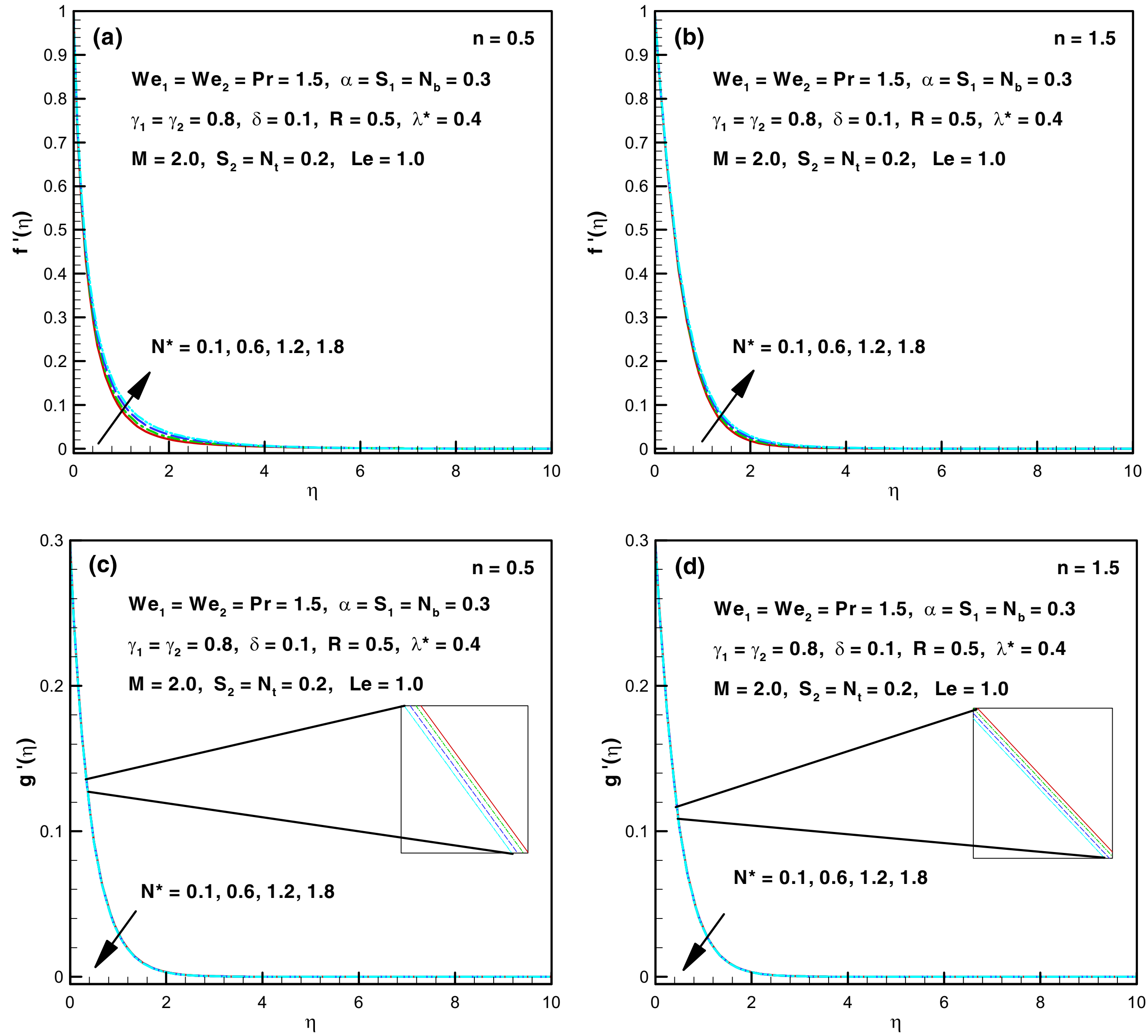

Fig. 4 **a–d** Impact of N^* on $f'(\eta)$ and $g'(\eta)$

b, it is reported that the higher N_t also enhances the liquid temperature. As thermophoresis is a mechanism wherein minor elements are dragged away from the hot to cold surface. Therefore, an enormous quantity of nanoparticles is transferred away from the intense surface which increases the temperature of the liquid.

6.6 Impact of R on $\theta(\eta)$

The characteristics of thermal radiation for ($n = 0.5$ and 1.5) is exposed in Fig. 11a, b on nanoliquid temperature field. There is an augmentation in both the liquid temperature and thermal thickness of boundary layer for the advance value of R. Increase in R heightens the heat flux from the sheet which contributes to rise in the liquid temperature. Moreover, we can also say that the coefficient of mean absorption decays for enhancing values of R which intensifies the temperature field.

6.7 Impact of γ_2 and S_2 on $\varphi(\eta)$

An intensification in nanoparticles concentration Biot number γ_2 and stratification parameter S_2 for shear thinning/thickening parameters is exposed in Figs. 12a, b and 13a,

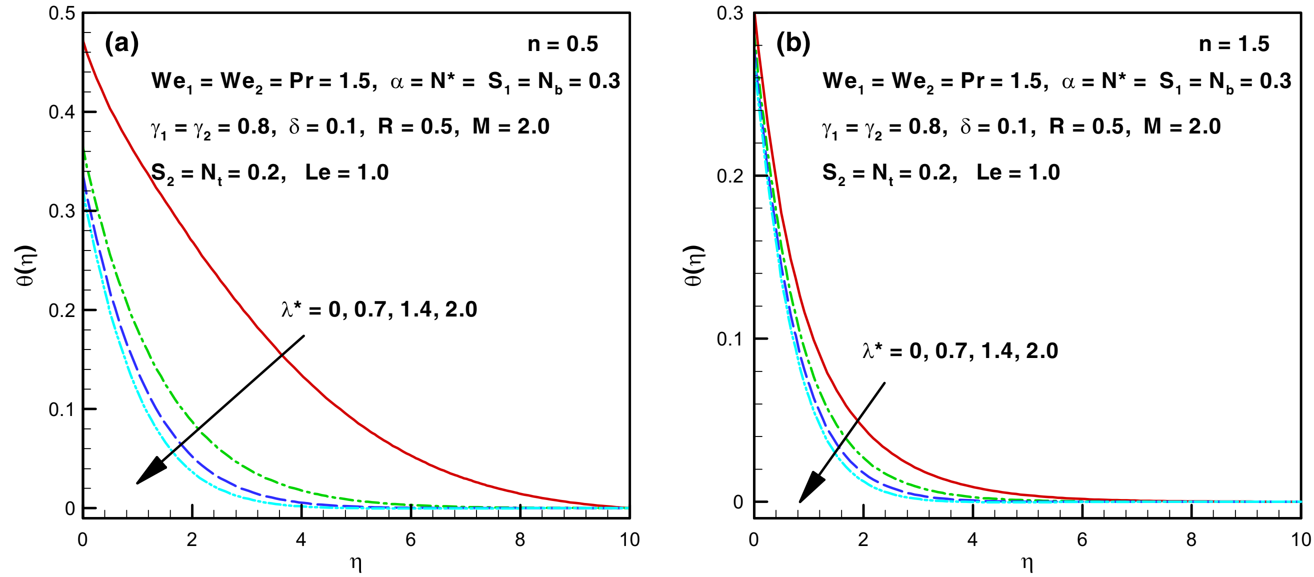

Fig. 5 **a**, **b** Impact of λ^* on $\theta(\eta)$.

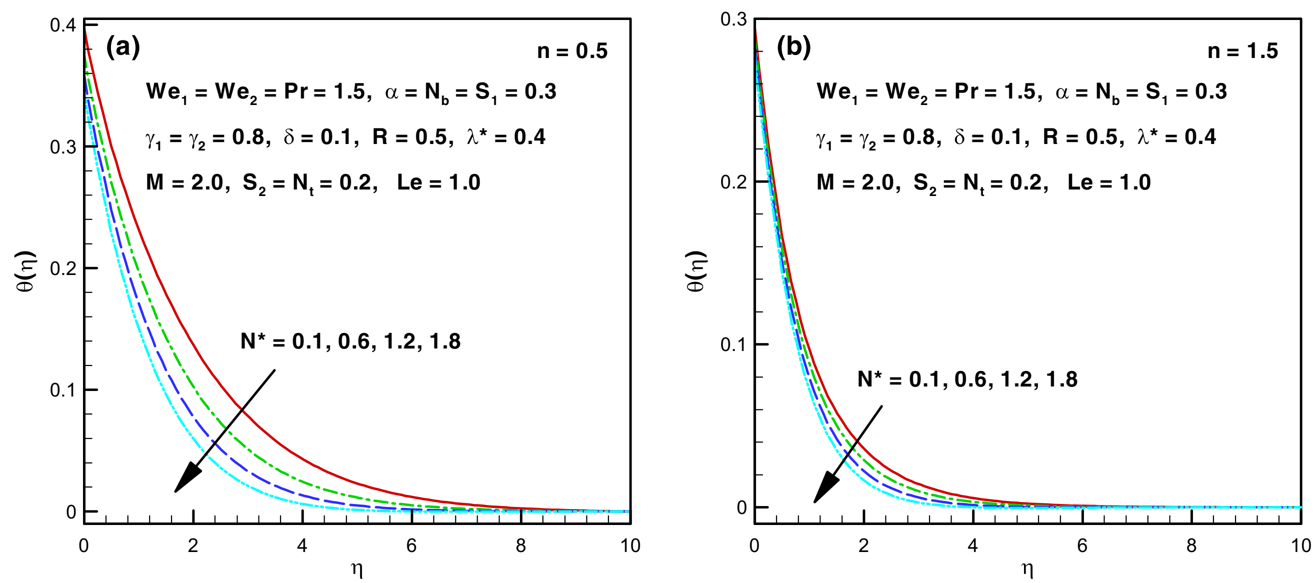

Fig. 6 **a**, **b** Impact of N^* on $\theta(\eta)$.

b. These graphs spectacle opposing behavior for higher value of these parameters. Increase in mass Biot number γ_2 enhances the concentration of nanoliquid; however, it declines for mass stratification parameter S_2. The higher values of γ_2 relate to sophisticated mass transfer coefficient and thus, the concentration field rises. On the other hand, it is inspected that when we enhances S_2, the difference between surface and reference nanoparticles reduces and the results in the declines of concentration field.

6.8 Tables of local skin friction coefficients, local Nusselt and Sherwood numbers

Tables 1 and 2 are established to show the tendency of the involved parameters on the local skin friction coefficients $\left(\frac{1}{2}C_{fx}Re_x^{\frac{1}{2}}, \frac{1}{2}\left(\frac{U_w}{V_w}\right)C_{fy}Re_x^{\frac{1}{2}}\right)$, local Nusselt number $\left(Re_x^{-\frac{1}{2}}Nu_x\right)$ and local Sherwood number $\left(Re_x^{-\frac{1}{2}}Sh_x\right)$ for

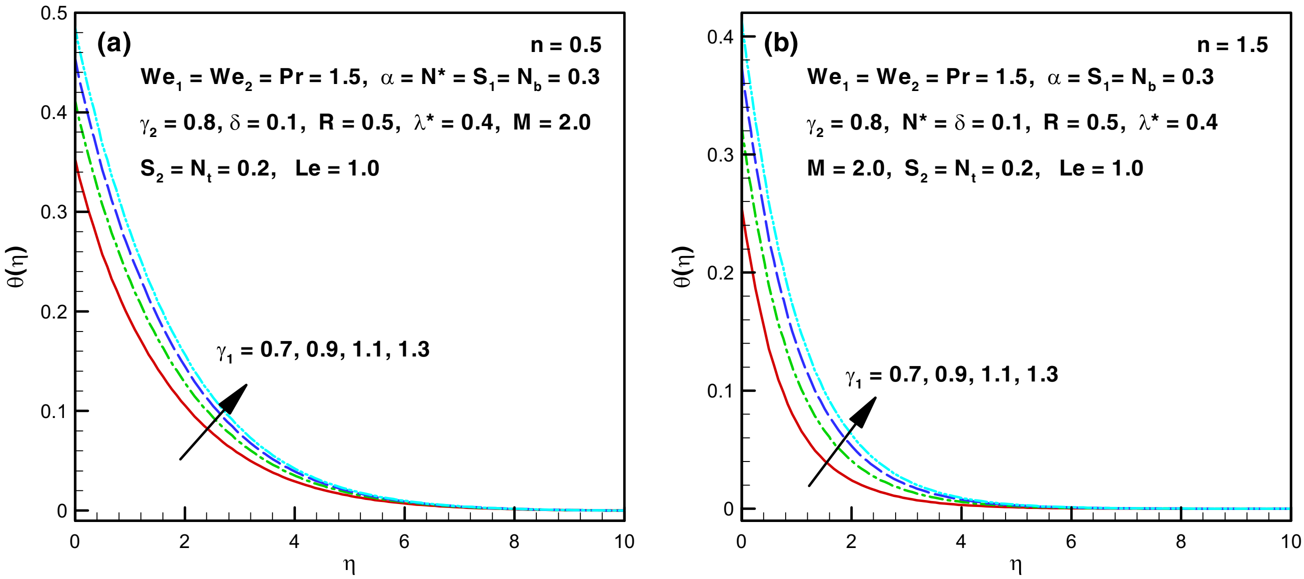

Fig. 7 **a**, **b** Impact of γ_1 on $\theta(\eta)$

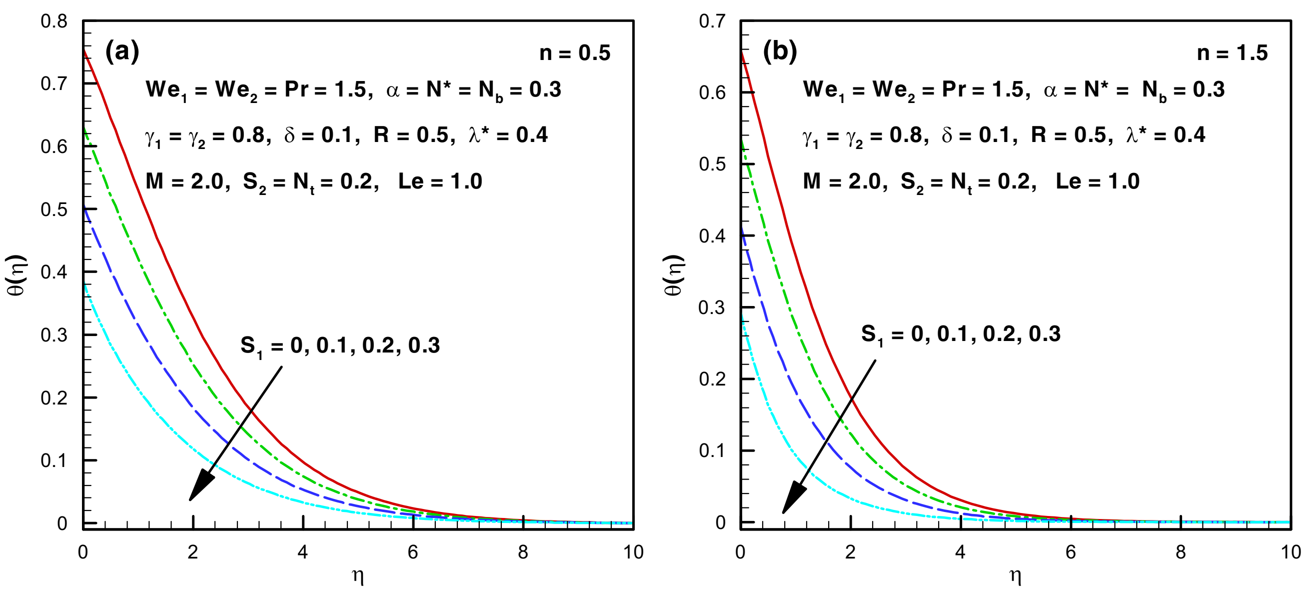

Fig. 8 **a**, **b** Impact of S_1 on $\theta(\eta)$

both shear thinning/thickening liquids. In Table 1, it is fascinating to note that by increasing the values of M, S_1 and S_2 the skin friction coefficient $\left(\frac{1}{2}C_{fx}Re_x^{\frac{1}{2}}\right)$ rises while it declines for enhancing values of λ^*, N^*, γ_1 and γ_2 for both $(n < 1)$ and $(n > 1)$. It is also noted that the skin friction coefficient $\left(\frac{1}{2}\left(\frac{U_w}{V_w}\right)C_{fy}Re_x^{\frac{1}{2}}\right)$ enhance for M, λ^*, N^*, γ_1 and γ_2, whereas conflicting behavior is being identified for S_1 and S_2. In Table 2, the rate of heat transfer is intensify for λ^*, N^*, γ_1, S_1 and S_2 and decline for M and γ_2. Moreover, the mass transfer rate for shear thinning/thickening liquids diminished for progressive values of λ^*, N^* and S_1 while augmented for M, γ_1 and γ_2.

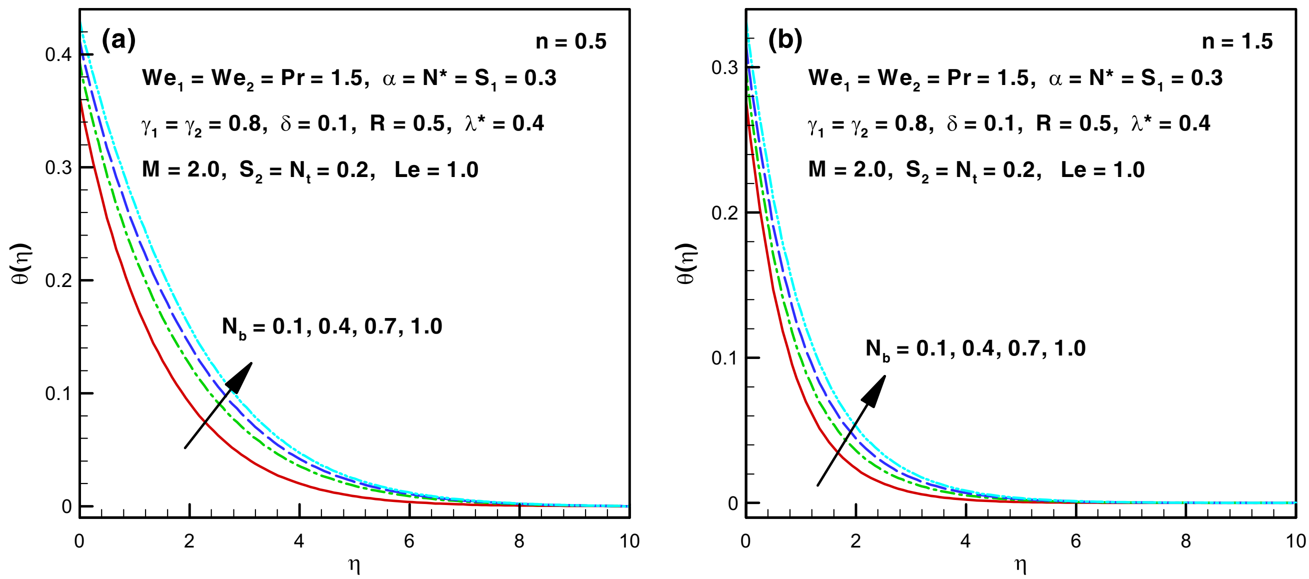

Fig. 9 **a**, **b** Impact of N_b on $\theta(\eta)$

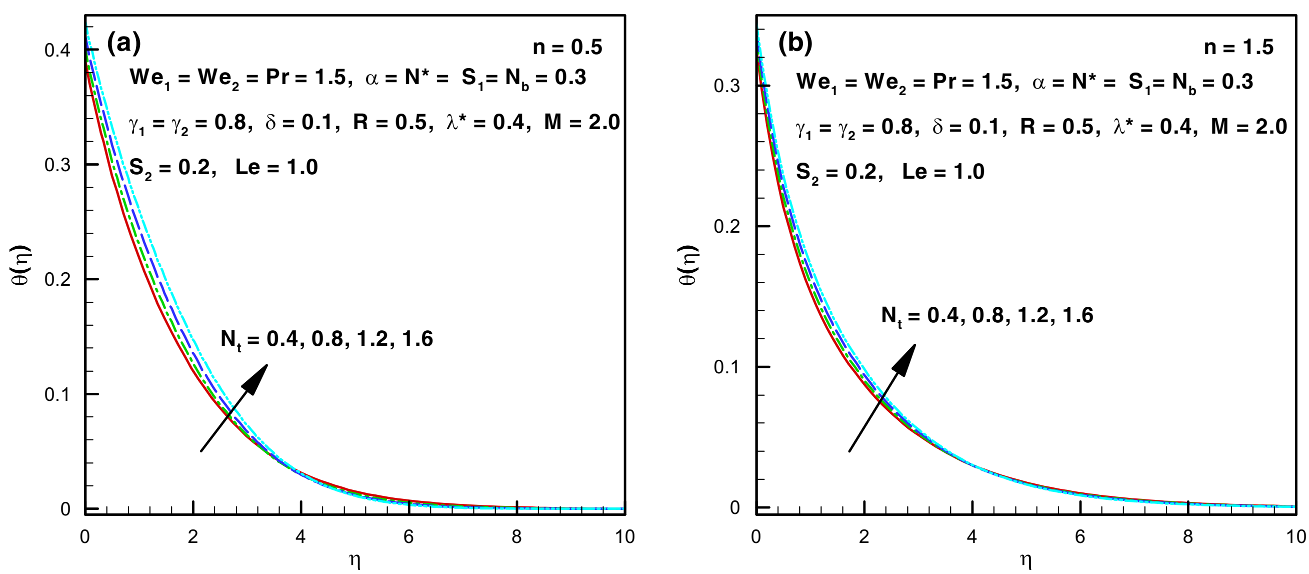

Fig. 10 **a**, **b** Impact of the N_t on $\theta(\eta)$

6.9 Authentication with former upshots

For the endorsement of numerical upshots of $-f''(0)$ and $-g''(0)$ with former related prose for diverse values of α, Tables 3 and 4 are organized. It is reported that intensifying values of α heighten $-f''(0)$ and $-g''(0)$. From these tables, a noteworthy agreement is being noted with earlier studies.

7 Main findings

Here we disclosed the properties of combined convective and stratification phenomena on 3D mixed convection flow of Carreau magnetite nanofluid with the impact of thermal radiation and the heat sink/source. The planned vision of this study is enumerated below:

- Both the liquid velocities $f'(\eta)$ and $g'(\eta)$ declined for higher magnetic parameter M, but the influence of

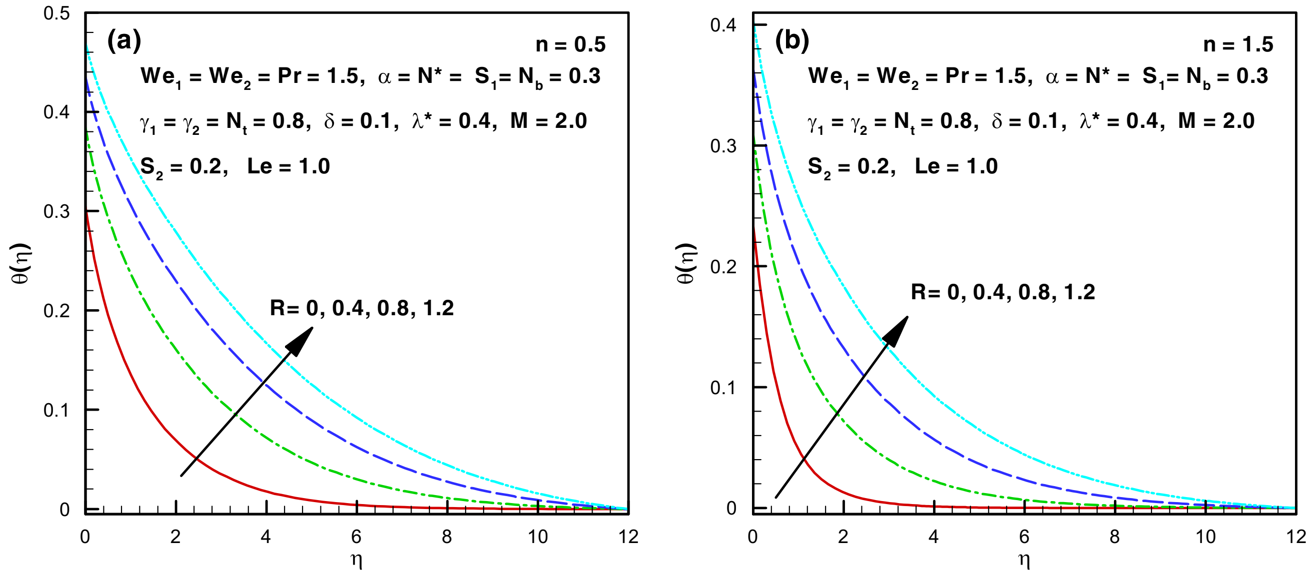

Fig. 11 **a**, **b** Impact of R on $\theta(\eta)$

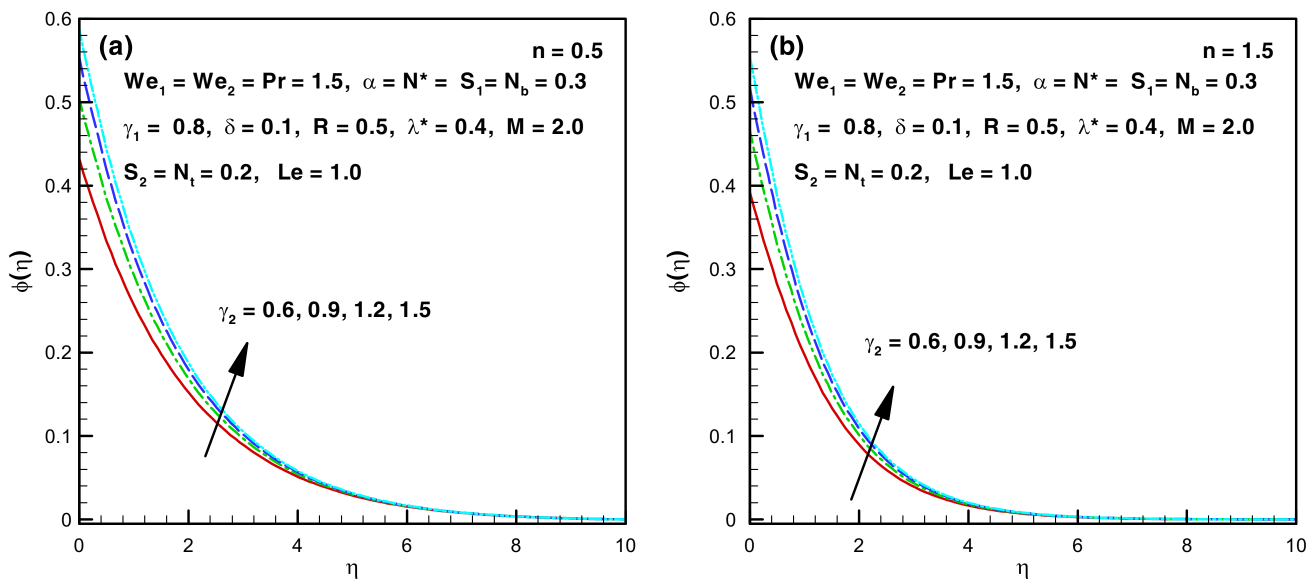

Fig. 12 **a**, **b** Impact γ_2 on $\varphi(\eta)$

mixed convection parameter λ^* was absolutely conflicting on velocity fields for both $(n < 1)$ and $(n > 1)$.

- The temperature field intensified for thermal Biot number γ_1 and thermal radiation parameter R, while it decayed for thermal stratification parameter S_1 for both shear thinning/thickening instances.
- The progressive values of mixed convection parameter λ^* diminished the liquid temperature and its allied thickness of the boundary layer, whereas it enhanced for Brownian motion N_b and thermophoresis parameter N_t.
- Quite opposite tend was being noted for advance values of mass stratification S_2 and mass Biot number γ_2 for both cases $(n = 0.5)$ and $(n = 1.5)$ on concentration field.

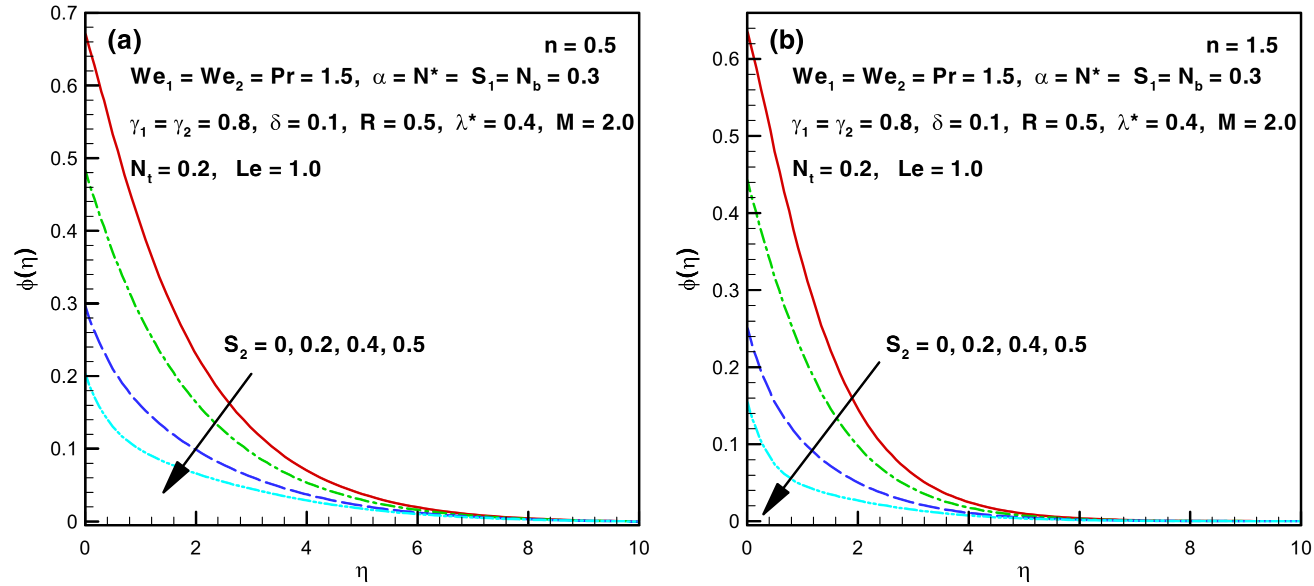

Fig. 13 **a**, **b** Impact of S_2 on $\varphi(\eta)$

Table 1 Numerical outcomes of skin friction coefficients when $We_1 = We_2 = Pr = 1.5, \delta = 0.1$, $N_t = 0.2, \alpha = N_b = 0.3, R = 0.5$, and $Le = 1.0$ are fixed

M	λ^*	N^*	S_1	γ_1	S_2	γ_2	$\frac{1}{2}C_{fx}Re_x^{\frac{1}{2}}$		$\frac{1}{2}\left(\frac{U_w}{V_w}\right)C_{fy}Re_x^{\frac{1}{2}}$	
							$n = 0.5$	$n = 1.5$	$n = 0.5$	$n = 1.5$
0.4	0.4	0.3	0.3	0.8	0.2	0.8	−1.449886	−2.677863	−0.2743207	−0.3103766
0.7							−1.707612	−3.330769	−0.3293321	−0.3809882
1.0							−2.089718	−4.382541	−0.403704	−0.4833723
1.3							−2.577088	−5.871595	−0.4926472	−0.6152907
0.4	0.1						−1.529535	−2.805652	−0.2731797	−0.3099874
	0.6						−1.399649	−2.593553	−0.2750317	−0.3106625
	1.2						−1.260903	−2.350347	−0.2769521	−0.3115580
	0.4	0.2					−1.459606	−2.695527	−0.2741636	−0.3102955
		0.4					−1.440249	−2.660300	−0.2744759	−0.3104574
		0.6					−1.421218	−2.625479	−0.2747809	−0.3106181
		0.3	0.0				−1.321206	−2.380301	−0.2779211	−0.3131885
			0.1				−1.364302	−2.479074	−0.2767067	−0.3122286
			0.2				−1.407209	−2.578299	−0.2755061	−0.3112912
			0.3	0.3			−1.539487	−2.868080	−0.2722469	−0.3089934
				0.5			−1.494958	−2.774491	−0.2732863	−0.3096711
				0.7			−1.462828	−2.705782	−0.2740254	−0.3101721
				0.8	0.0		−1.428643	−2.629172	−0.2748222	−0.3107542
					0.1		−1.439262	−2.653488	−0.2745713	−0.3105650
					0.3		−1.460514	−2.702294	−0.2740706	−0.3101889
					0.2	0.2	−1.471351	−2.721165	−0.2739385	−0.3101314
						0.4	−1.462498	−2.703455	−0.2740963	−0.3102313
						0.6	−1.455524	−2.689352	−0.2742204	−0.3103113

Table 2 Numerical outcomes of local Nusselt and Sherwood numbers when $We_1 = We_2 = \mathrm{Pr} = 1.5, \delta = 0.1$, $N_t = 0.2, \alpha = N_b = 0.3, R = 0.5$, and $Le = 1.0$ are fixed

M	λ^*	N^*	S_1	γ_1	S_2	γ_2	$Re_x^{-\frac{1}{2}} Nu_x$		$Re_x^{-\frac{1}{2}} Sh_x$	
							$n = 0.5$	$n = 1.5$	$n = 0.5$	$n = 1.5$
0.4	0.4	0.3	0.3	0.8	0.2	0.8	0.850012	0.884927	0.317179	0.294267
0.7							0.826654	0.870377	0.332508	0.303815
1.0							0.792856	0.850188	0.354688	0.317064
1.3							0.750506	0.826037	0.382480	0.332913
0.4	0.1						0.845825	0.885076	0.319927	0.294169
	0.6						0.852716	0.885178	0.315405	0.294102
	1.2						0.859953	0.886596	0.310656	0.293171
	0.4	0.2					0.849308	0.884727	0.317642	0.294398
		0.4					0.850704	0.885127	0.316726	0.294136
		0.6					0.852049	0.885526	0.315843	0.293873
		0.3	0.0				0.684003	0.704523	0.608747	0.589510
			0.1				0.728453	0.752408	0.510368	0.490156
			0.2				0.782426	0.811008	0.413180	0.391744
			0.3	0.3			0.457360	0.470288	0.074621	0.051996
				0.5			0.649193	0.671899	0.193348	0.169506
				0.7			0.791674	0.822863	0.281244	0.257853
				0.8	0.0		0.849427	0.883309	0.254051	0.236263
					0.1		0.849719	0.884117	0.282108	0.262043
					0.3		0.850306	0.885740	0.362270	0.335695
					0.2	0.2	0.857226	0.893112	0.312446	0.288895
						0.4	0.854273	0.889776	0.314384	0.291084
						0.6	0.851925	0.887114	0.315924	0.292832

Table 3 An assessment table of $-f''(0)$ in limiting sense when $We_1 = We_2 = M = \lambda^* = N^* = 0$ and $n = 1$ are fixed

$-f''(0)$					
α	Ref. [39]	Ref. [40]	Ref. [41]		Present (bvp4c)
			(bvp4c)	(HAM)	
0.0	1	1	1	1	1
0.25	1.048813	1.048813	1.0488130	1.0488131	1.0488113
0.50	1.093097	1.093096	1.0930954	1.0930943	1.0930949
0.75	1.134485	1.134486	1.1344854	1.1344858	1.1344856
1.0	1.173720	1.173721	1.1737199	1.1737201	1.1737208

Table 4 An assessment table of $-g''(0)$ in limiting sense when $We_1 = We_2 = M = \lambda^* = N^* = 0$ and $n = 1$ are fixed

$-g''(0)$					
α	Ref. [39]	Ref. [40]	Ref. [41]		Present (bvp4c)
			(bvp4c)	(HAM)	
0.0	0	0	0	0	0
0.25	0.194564	0.194565	0.1945652	0.1945617	0.19456397
0.50	0.465205	0.465206	0.4652058	0.4652047	0.46520490
0.75	0.794622	0.794619	0.7946180	0.7946184	0.79461824
1.0	1.173720	1.173721	1.1737199	1.1737201	1.17372080

References

1. Choi SUS (1995) Enhancing thermal conductivity of fluids with nanoparticles. ASME Int Mech Eng 66:99–105
2. Mahanthesh B, Gireesha BJ, Gorla RSR, Abbasi FM, Shehzad SA (2016) Numerical solutions for magnetohydrodynamic flow of nanofluid over a bidirectional non-linear stretching surface with prescribed surface heat flux boundary. J Magn Magn Mater 417:189–196
3. Hayat T, Rashid M, Imtiaz M, Alsaedi A (2017) MHD convective flow due to a curved surface with thermal radiation and chemical reaction. J Mol Liq 225:482–489
4. Khan M, Irfan M, Khan WA (2017) Numerical assessment of solar energy aspects on 3D magneto-Carreau nanofluid: a revised proposed relation. Int J Hydrog Energy 42:22054–22065
5. Hayat T, Khan MI, Waqas M, Alsaedi A, Khan MI (2017) Radiative flow of micropolar nanofluid accounting thermophoresis and Brownian moment. Int J Hydrog Energy 42:16821–16833
6. Upadhya SM, Raju CSK (2017) Multiple slips on magnetohydrodynamic Carreau dustynano fluid over a stretched surface with Cattaneo–Christov heat flux. J Nanofluids 1:1074–1108
7. Mahanthesh B, Mabood F, Gireesha BJ, Gorla RSR (2017) Effects of chemical reaction and partial slip on the three-dimensional flow of a nanofluid impinging on an exponentially stretching surface. Eur Phys J Plus. https://doi.org/10.1140/epjp/i2017-11389-8
8. Mahanthesh B, Gireesha BJ, Raju CSK (2017) Cattaneo–Christov heat flux on UCM nanofluid flow across a melting surface with double stratification and exponential space dependent internal heat source. Inf Med Unlocked 9:26–34

9. Anwar MS, Rasheed A (2017) Simulations of a fractional rate type nanofluid flow with non-integer Caputo time derivatives. Comput Math Appl 74:2485–2502
10. Raju CSK, Sandeep N (2017) Unsteady Casson nanofluid flow over a rotating cone in a rotating frame filled with ferrous nanoparticles: a numerical study. J. Magn Magn Mater 421:216–224
11. Mustafa M, Khan JA, Hayat T, Alsaedi A (2017) Buoyancy effects on the MHD nanofluid flow past a vertical surface with chemical reaction and activation energy. Int J Heat Mass Transf 108:1340–1346
12. Haq RU, Rashid I, Khan ZA (2017) Effects of aligned magnetic field and CNTs in two different base fluids over a moving slip surface. J Mol Liq 243:682–688
13. Hayat T, Khan MI, Waqas M, Alsaedi A, Farooq M (2017) Numerical simulation for melting heat transfer and radiation effects in stagnation point flow of carbon–water nanofluid. Comput Methods Appl Mech Eng 315:1011–1024
14. Irfan M, Khan M, Khan WA (2017) Numerical analysis of unsteady 3D flow of Carreau nanofluid with variable thermal conductivity and heat source/sink. Results Phys 7:3315–3324
15. Raju CSK, Hoque MM, Anika NN, Mamatha SU, Sharma P (2017) Natural convective heat transfer analysis of MHD unsteady Carreau nanofluid over a cone packed with alloy nanoparticles. Powder Tech 317:408–416
16. Hayat T, Rashid M, Alsaedi A, Ahmad B (2018) Flow of nanofluid by nonlinear stretching velocity. Results Phys 8:1104–1109
17. Zeeshan A, Shezhad N, Ellahi R (2018) Analysis of activation energy in Couette–Poiseuille flow of nanofluid in the presence of chemical reaction and convective boundary conditions. Results Phys 8:502–512
18. Upadhya SM, Raju CSK (2018) Comparative study of Eyring and Carreau fluids in a suspension of dust and nickel nanoparticles with variable conductivity. Eur Phys J Plus. https://doi.org/10.1140/epjp/i2018-11979-x
19. Mukhopadhyay S, Ishak A (2012) Mixed convection flow along a stretching cylinder in a thermally stratified medium. J Appl Math https://doi.org/10.1155/2012/491695
20. Mahanthesh B, Gireesha BJ, Gorla RSR (2016) Heat and mass transfer effects on the mixed convective flow of chemically reacting nanofluid past a moving/stationary vertical plate. Alex Eng J 55:569–581
21. Imtiaz M, Hayat T, Alsaedi A (2016) Mixed convection flow of Casson nanofluid over a stretching cylinder with convective boundary conditions. Adv Powder Tech 27:2245–2256
22. Waqas M, Khan MI, Hayat T, Alsaedi A (2017) Stratified flow of an Oldroyd-B nanoliquid with heat generation. Results Phys 7:2489–2496
23. Besthapu P, Haq RU, Bandari S, Al-Mdallal QM (2017) Mixed convection flow of thermally stratified MHD nanofluid over an exponentially stretching surface with viscous dissipation effect. J Taiwan Inst Chem Eng 71:307–314
24. Ibrahim SM, Lorenzini G, Kumar PV, Raju CSK (2017) Influence of chemical reaction and heat source on dissipative MHD mixed convection flow of a Casson nanofluid over a nonlinear permeable stretching sheet. Int J Heat Mass Transf 111:346–355
25. Khan MI, Waqas M, Hayat T, Khan MI, Alsaedi A (2017) Behavior of stratification phenomenon in flow of Maxwell nanomaterial with motile gyrotactic microorganisms in the presence of magnetic field. Int J Mech Sci 131–132:426–434
26. Hashim, Hamid A, Khan M (2018) Unsteady mixed convective flow of Williamson nanofluid with heat transfer in the presence of variable thermal conductivity and magnetic field. J Mol Liq 260:436–446
27. Waqas M, Farooq M, Khan MI, Alsaedi A, Hayat T, Yasmeen T (2016) Magnetohydrodynamic (MHD) mixed convection flow of micropolar liquid due to nonlinear stretched sheet with convective condition. Int J Heat Mass Transf 102:766–772
28. Mamatha SU, Raju CSK, Makinde OD (2017) Effect of convective boundary condition on MHD Carreau dusty fluid over a stretching sheet with heat source. Defect Diffus Forum 377:233–241
29. Mahanthesh B, Gireesha BJ, Athira PR (2017) Radiated flow of chemically reacting nanoliquid with an induced magnetic field across a permeable vertical plate. Results Phys 7:2375–2383
30. Hayat T, Rafique K, Muhammad T, Alsaedi A (2018) Carbon nanotubes significance in Darcy–Forchheimer flow. Results Phys 8:26–33
31. Hayat T, Rashid M, Alsaedi A (2018) Three dimensional radiative flow of magnetite-nanofluid with homogeneous-heterogeneous reactions. Results Phys 8:268–275
32. Irfan M, Khan M, Khan WA, Ayaz M (2018) Modern development on the features of magnetic field and heat sink/source in Maxwell nanofluid subject to convective heat transport. Phys Lett A 382:1992–2002
33. Upadhya SM, Raju CSK, Saleem S (2018) Nonlinear unsteady convection on micro and nanofluids with Cattaneo–Christov heat flux. Results Phys 9:779–786
34. Irfan M, Khan M, Khan WA (2018) Interaction between chemical species and generalized Fourier's law on 3D flow of Carreau fluid with variable thermal conductivity and heat sink/source: a numerical approach. Results Phys 10:107–117
35. Carreau PJ (1972) Rheological equations from molecular network theories. Trans Soc Rheol 16:99–127
36. Gireesha BJ, Kumar PBS, Mahanthesh B, Shehzad SA, Rauf A (2017) Nonlinear 3D flow of Casson–Carreau fluids with homogeneous–heterogeneous reactions: a comparative study. Results Phys 7:2762–2770
37. Khan M, Irfan M, Khan WA, Alshomrani AS (2017) A new modeling for 3D Carreau fluid flow considering nonlinear thermal radiation. Results Phys 7:2692–2704
38. Upadhya SM, Raju CSK (2018) Unsteady flow of Carreau fluid in a suspension of dust and graphene nanoparticles with Cattaneo–Christov heat flux. J Heat Transf. https://doi.org/10.1115/1.4039904
39. Wang CY (1984) The three dimensional flow due to a stretching flat surface. Phys Fluids 27:1915–1917
40. Liu IC, Anderson HI (2008) Heat transfer over a bidirectional stretching sheet with variable thermal conditions. Int J Heat Mass Transf 51:4018–4024
41. Khan M, Irfan M, Khan WA (2017) Impact of forced convective radiative heat and mass transfer mechanisms on 3D Carreau nanofluid: a numerical study. Eur Phys J Plus. https://doi.org/10.1140/epjp/i2017-11803-3